

# ON THE SEPARATION BETWEEN BARYONIC AND DARK MATTER: EVIDENCE FOR PHANTOM DARK MATTER?

ALEXANDER KNEBE<sup>1</sup>, CLAUDIO LLINARES<sup>2</sup>, XUFEN WU<sup>3</sup> HONGSHENG ZHAO<sup>3,4</sup>

(Dated: Submitted Version ...)  
Draft version November 19, 2018

## ABSTRACT

The recent years have seen combined measurements of X-ray and (weak) lensing contours for colliding galaxy clusters such as, for instance, the famous “Bullet” cluster. These observations have revealed offsets in the peaks of the baryonic and (dominant) gravitational matter component of order  $\sim 100 - 200$  kpc. Such discrepancies are difficult to explain using modified theories for gravity other than dark matter. Or are they not? Here we use the concept of “phantom dark matter” that is based upon a Newtonian interpretation of the MONDian gravitational potential. We show that this idea is in fact capable of producing substantial offsets in idealistic density configurations, involving a uniform external field. However, when analysed in a MONDian cosmological framework we deduce that the size (and probability) of the effect is too small to explain the observed offsets found in the most recent observations, at least in the simplest incarnation of phantom dark matter as discussed here. The lensing centers in merging galaxy clusters are likely very close to the centers of true mass even in a MONDian cosmology. This gives the support to the idea that neutrino-like non-collisional matter might be responsible for the observed offsets of lensing and X-ray peaks.

*Subject headings:* galaxies: evolution – galaxies: halos – cosmology: theory – cosmology: dark matter  
– methods:  $N$ -body simulations

## 1. INTRODUCTION

The standard  $\Lambda$  Cold Dark Matter ( $\Lambda$ CDM) model (cf., Komatsu et al. 2008) explains the formation of cosmological structure in the non-linear regime in a hierarchical way, i.e. big structures are not formed monolithically but by successive merging of small structures (e.g., Davis et al. 1985). Recent cosmological simulations also support this idea of hierarchical structure formation in MOND gravity (Llinares et al. 2008) (but see also the analytical models of Sanders (2008) and Zhao et al. (2008)). The hierarchical merging scenario naturally promotes the picture that we should observe collisions of (clusters of) galaxies. Observationally there is evidence that some of these impacts actually occur with speeds that are not readily reproduced by simulations of  $\Lambda$ CDM structure formation, in the sense that the relative speed of the merging dark halos is rarely very higher than the internal dispersion of each halo (Hayashi & White 2006; Knebe et al. 2008; Llinares et al. 2008; Angus & McGaugh 2008). There is, for instance, the famous “Bullet cluster”, an extremely high velocity merger between two galaxy clusters, with an inferred shock velocity of  $\sim 4700$  km/sec. While relative encounters with comparable velocities are rather rare in pure dark matter simulations (e.g. Hayashi & White 2006; Knebe et al. 2008), they may nevertheless be accommodated when considering explicit hydrodynamical

modelling of the phenomenon (Springel & Farrar 2007).

One unavoidable consequence of any high speed collision of mass concentrations seems to be the decoupling or offsetting of the baryonic component from the dark component. Aside from the aforementioned Bullet cluster – whose offset has been measured to be approximately  $\sim 100$  kpc (e.g. Clowe et al. 2006) – more examples are given in Jee et al. (2005a), Jee et al. (2005b), and Bradač et al. (2008). The latter authors actually present data for a particular cluster (i.e. MACS J0025.4-1222) with an even greater difference of  $\sim 200$  kpc in the peak of the baryonic and the dark matter. All this work is culminated in one particular recent *Letter* by Shan et al. (2009) where a sample of 38 galaxy clusters has been studied utilizing both X-ray and strong lensing observations. They show that such offsets are a common phenomenon in galaxy clusters: they found at least 13 objects with a separation greater than 50 kpc with 3 clusters exhibiting a separation between baryonic and (hypothetic) dark component in excess of 200 kpc.

All these papers are analysing combined X-ray and lensing observations to decipher (and actually measure) the offset between baryonic and dark matter. But how certain are we that the lensing signal is caused by “real” dark matter particles? What if the gravitational potential is not generated by Newtonian physics yet interpreted in that way?

One theory capable of producing potentials akin to dark matter particles is modified Newtonian dynamics (MOND, Milgrom 1983); (pedagogical) reviews of the concepts and successes can be found in, for instance, Sanders & McGaugh (2002) and Milgrom (2008). While MOND was originally proposed as an alternative to Newtonian gravity designed to solely explain galactic dynamics without the need for dark matter the theory has gained substantial momentum during the past decade:

<sup>1</sup> Departamento de Física Teórica, Modulo C-XI, Facultad de Ciencias, Universidad Autónoma de Madrid, 28049 Cantoblanco, Madrid, Spain

<sup>2</sup> Astrophysikalisches Institut Potsdam, An der Sternwarte 16, 14482 Postdam, Germany

<sup>3</sup> SUPA, University of St Andrews, North Haugh, Fife, KY16 9SS, UK

<sup>4</sup> Leiden University, Sterrewacht and Instituut-Lorentz, Niels-Bohrweg 2, 2333 CA, Leiden, The Netherlands

although current cosmological observations point to the existence of vast amounts of non-baryonic dark matter in the Universe (e.g. Komatsu et al. 2008), not all of the features of CDM models appear to match observational data (e.g., the “missing satellite problem” (Klypin et al. 1999; Moore et al. 1999) and the so-called “cusp-core crisis” (e.g. de Blok et al. 2003; Swaters et al. 2003)). Just as for CDM the MOND theory successfully matches observations on a wide range of scales, different types of galaxies including dwarfs and giants, spirals and ellipticals (Famaey & Binney 2005; Gentile et al. 2007; Milgrom & Sanders 2007; Milgrom 2007; Sanders & Noordermeer 2007; McGaugh 2008; Angus 2008). However, one of MOND’s major set-backs for a long time was the lack of a covariant formulation of the theory. This has been remedied by Bekenstein (2004) who was the first to cast MOND into a more universal form compliant with general relativity. This in turn spawned further investigations into the same direction leaving us nowadays with various relativistic formulations of the MOND theory (e.g. Bekenstein 2004; Sanders 2005; Bruneton & Esposito-Farèse 2007; Zhao 2007; Zlosnik et al. 2007; Zhao 2008; Skordis 2008; Blanchet & Le Tiec 2009); a recent review of both MOND and its relativistic offspring (in particular the *TeVēS* formulation of Bekenstein (2004)) can be found in Milgrom (2008) and Skordis (2009). We though need to acknowledge that despite the original idea of abandoning the need for dark matter, even MOND cannot do without it: despite the great success we need to accept that even MOND cannot do well without dark matter completely. A recent study utilizing a combination of strong and weak lensing by galaxy clusters indicates the necessity for neutrinos of mass  $5 - 7eV$  (Natarajan & Zhao 2008). And to be consistent with dark matter estimates of galaxy clusters and observations of the CMB anisotropies Angus (2009); Angus et al. (2009) claims for  $11eV$  neutrinos. One theory capable of accomodating both these requirements is that of a mass-varying neutrino by Zhao (2008). In summary, we are eventually left with a situation where the development of several frameworks for a relativistic formulation of MOND enabled the study of the cosmic microwave background (Skordis et al. 2006; Li et al. 2008), cosmological structure formation (Halle et al. 2008; Skordis 2008), strong gravitational lensing of galaxies (Zhao 2006; Chen & Zhao 2006; Shan et al. 2008), and weak lensing of clusters (Angus et al. 2007; Famaey et al. 2008). The MOND theory has matured and became a credible competitor to the commonly accepted CDM model.

In that regards, however, it appears important to look for even more tests that are capable of discriminating between MOND and Newtonian gravity, especially in the context of cosmology. We therefore raise the question whether the kinds of offsets alluded to above can be explained by simply interpreting the MONDian potential in a Newtonian way? This concept of “phantom dark matter” was originally introduced in the beginnings of MOND already by Milgrom (1986) and has recently been discussed by Milgrom (2008), Wu et al. (2008), and Bienaymé et al. (2009). It is based upon the idea to use the MONDian potential in a dark matter context, i.e. given the MONDian potential one can use the Newtonian Poisson’s equation to derive the corresponding den-

sity of matter that would be needed in the Newtonian context. Then, subtracting the visible (baryonic) matter one obtains the “virtual” dark matter or, in other words, “phantom dark matter” distribution predicted by MOND. And in a Newtonian interpretation this phantom dark matter would be responsible for the gravitational lensing signal alluded to above.

We though need to acknowledge that Brownstein & Moffat (2007) already pointed out the possibility that the observed offset in the (alleged) dark matter and baryonic density peaks of the Bullet cluster system can be explained by extending the equations for gravitational lensing to modified gravity, without the need for a dominant dark matter component. Further, as MOND is a non-linear theory it is not clear whether the (baryonic) matter will be distributed *ab initio* in the same way as phantom dark matter. We therefore set out to answer the question whether or not these two density fields share peaks at the same locations and are distributed in comparable ways, respectively. Can an offset between the dark and baryonic matter be explained by the non-linearity of the MONDian Poisson’s equation and the existence of this putative phantom matter, respectively?

We need to close with a cautionary note: this work does *not* deal with (collisions of) galaxies or galaxy clusters; we are solely focusing on the properties of the matter density fields and their respective peaks. The primary question we set out to answer is whether or not MOND will produce offsets between the actual (baryonic) matter component and the phantom matter field, even though this work is motivated by observations of such offsets in galaxy clusters.

## 2. THE NON-COSMOLOGICAL FRAMEWORK

Before investigating phantom dark matter in a cosmological environment we start off with phrasing the question about shifts in the respective density peaks for MONDian systems in a non-cosmological context. This will provide us with a gauge whether or not we should actually expect to find the reputed offsets.

### 2.1. Phantom Dark Matter

The MONDian Poisson’s equation embedded within an external field reads as follows

$$-\nabla \cdot \left[ \mu \left( \frac{|\mathbf{g}|}{a_0} \right) \mathbf{g} \right] = 4\pi G\rho, \quad \mathbf{g} = \mathbf{g}_{\text{ext}} - \nabla\Phi_{\text{int}}, \quad (1)$$

where  $\rho$  is the baryonic matter,  $\mathbf{g}_{\text{ext}}$  an external field, and  $\Phi_{\text{int}}$  the (internal) potential of the system and  $\mu(x)$  is  $\mu \rightarrow 1$  for  $x \gg 1$  (Newtonian limit) and  $\mu \rightarrow x$  for  $x \ll 1$  (deep MOND limit).<sup>5</sup> We now take the liberty to interpret this internal potential  $\Phi_{\text{int}}$  within the context of Newtonian gravity

$$\nabla^2\Phi_{\text{int}} = 4\pi G(\rho + \rho_{\text{ph}}), \quad (2)$$

where the  $(\rho + \rho_{\text{ph}})$  is the total dynamical mass of the system, and  $\rho_{\text{ph}}$  is the so called “phantom dark matter”, which can be held responsible for the “extra grav-

<sup>5</sup> Please note that we used  $\mu(x) = x(1+x^2)^{-1/2}$  as originally suggested by Milgrom (1983) throughout our tests.

TABLE 1  
PARAMETERS OF OUR NON-COSMOLOGICAL TEST MODEL. THE MASS IS IN UNIT OF ( $10^{10} M_{\odot}$ ), POSITIONS AND  $r_0$  ARE IN UNITS OF  $kpc$ , AND THE EXTERNAL GRAVITY ACCELERATION IS IN UNIT OF  $a_0$ .

Model	Mass	Centre	$g_{\text{ext}}$	$r_0$
G+EF	10.0	(0,0,0)	1.0	2.0

ity beyond the baryonic matter”<sup>6</sup> in the linear Poisson’s equation Eq. (2). But as opposed to the dark matter theory, MOND immediately predicts the distribution of the dynamical mass as soon as the baryons  $\rho$  and the gravity of the environment  $\mathbf{g}_{\text{ext}}$  are specified. However, due to the external field  $\mathbf{g}_{\text{ext}}$  the boundary condition of the (internal) system changes, not necessarily preserving spherical symmetry: the distribution of the dynamical mass is somewhat different from that of CDM halos (see Wu et al. 2007, 2008). Further, there exist negative solutions of the phantom dark matter, and the peaks of dynamical mass can in fact be offset to the baryonic peaks! These effects are most significant at places where the external and internal fields are comparable and should be quantified more carefully in the following subsection.

## 2.2. The Simulations

For the non-cosmological settings studied in this Section we use the MONDian Poisson solver developed by the Bologna group (Ciotti et al. 2006; Nipoti et al. 2007) to solve Eq. (1) and hence derive the internal potential  $\Phi_{\text{int}}$  of the systems under investigation. The Poisson solver is a spherical grid code, and our choice for the grid parameters is  $n_r \times n_{\theta} \times n_{\phi} = 256 \times 64 \times 128$  with a radial grid spacing given by  $r_i = r_0 \tan[(i + 0.5)0.5\pi/(n_r + 1)]$  kpc. We further utilize Eq. (2) to derive the dynamical mass and the phantom matter, respectively.

All our (baryonic) galaxies have a Plummer density profile

$$\rho(r) = \left( \frac{3M}{4\pi b^3} \right) \left( 1 + \frac{r^2}{b^2} \right)^{-5/2}, \quad (3)$$

with a core radius  $b$  of 1.0 kpc.

We investigated several scenarios (cf. discussion below in Section 2.3), however, decided to only present the results for one representative configuration where a single galaxy G is embedded within a strong constant external field EF. A summary of the actual parameters of the model can be found Table 1.

## 2.3. Density Peak Offsets

Figure 1 shows the distribution of the dynamical mass for model G+EF, i.e. a single galaxy embedded within an external field of strength  $|\mathbf{g}_{\text{ext}}| = a_0$  along the  $x$ -axis. We notice that when the internal and external field are of the same order of magnitude, i.e. at  $x \approx 15$  kpc there are some noticeable effects: first, we obtain negative dynamical mass on the corners perpendicular to the direction of external field also mentioned by Milgrom (1986) and

<sup>6</sup> Or in other words “dark matter”.

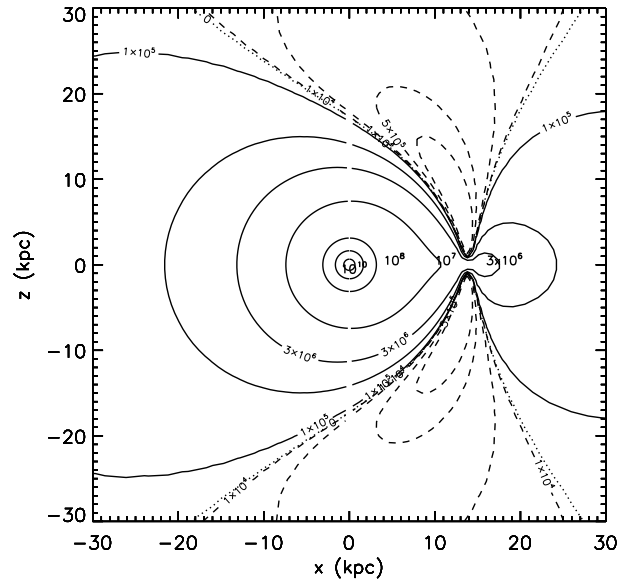


FIG. 1.— Isodensity contours of the dynamical mass, i.e. baryons + phantom dark matter density, on the  $x - z$  plane for a galaxy embedded within an external field along the  $x$ -axis.

Wu et al. (2008); second, there exist an additional peak on the  $x$ -axis, right where the external and internal fields cancel each other! However, this additional peak is four orders of magnitude smaller than the baryonic peak.

We have also run idealistic simulations with (un-)equal mass galaxies with and without external fields (not shown though). In summary, we have seen that in most of the situations the interpretation of the MONDian potential in a Newtonian sense will lead to the prediction of additional peaks in the distribution of the dynamical mass when compared to the actual (underlying) baryonic matter distribution. However, the strength of these extra peaks vary and depend on the actual setup of the system ranging from as low as four orders of magnitude smaller to as large as 1% for the cases considered here.

Encouraged by the observation that we actually recover offsets in our controlled experiments we may now rightfully ask the question *whether these additional phantom peaks occur in realistic cosmological simulations*, i.e., whether a self-consistent cosmological simulation will provide a suitable variety of configurations so that we will in fact be able to observe (and quantify) the offset between the baryonic and phantom matter peaks.

## 3. THE COSMOLOGICAL FRAMEWORK

### 3.1. Phantom Dark Matter

The equation for the (MONDian) gravitational potential in a cosmological setting is somewhat different to Eq. (1) and reads

$$\nabla \cdot \left[ \mu \left( \frac{|\nabla \Phi_M|}{a\gamma(a)} \right) \nabla \Phi_M \right] = \frac{4\pi G}{a} (\rho - \bar{\rho}), \quad (4)$$

We further took the liberty to encode the MONDian acceleration scale  $\gamma(a)$  as a (possible) function of the cosmic expansion factor  $a$ . The most naive choice would be  $\gamma(a) = g_0 = 1.2 \times 10^{-8} \text{cm/sec}^2$  whereas other theories may lead to different dependencies; for instance, in Zhao (2008)  $\gamma(a)$  is given as  $\gamma(a) = a^{1/2} g_0$ . For more details and a derivation of this equation we refer the reader

to Llinares et al. (2008) where it has been justified and implemented into the cosmological  $N$ -body code MLAPM (Knebe et al. 2001).

Given the MONDian potential  $\Phi_M$  we may now apply the same logic as in Section 2 and use it with the Newtonian Poisson's equation whose right-hand-side will again no longer be the (baryonic) density  $\rho$  field alone but rather read as follows

$$\nabla \cdot [\nabla \Phi_M] = \frac{4\pi G}{a} \left[ (\rho + \rho_{\text{ph}}) - \overline{(\rho + \rho_{\text{ph}})} \right]. \quad (5)$$

This is the defining equation for the phantom matter density field  $\rho_{\text{ph}}$  used throughout this Section.

### 3.2. The Simulation

The analysis presented in here is based upon a particular simulation published in Llinares et al. (2008), i.e. the OCBMond2 model. This simulation has been run in a cosmological volume with a side length of  $32h^{-1}\text{Mpc}$  and utilized  $128^3$  particles. It employed the MONDification of the  $N$ -body code MLAPM (Knebe et al. 2001; Llinares et al. 2008). We chose to simulate an open universe with neither dark matter nor dark energy but characterized by  $\Omega_b = 0.04$ . The simulation was started at redshift  $z = 50$  and resorted to a Hubble parameter of  $h = 0.7$ . We further need to mention that there are two values  $\sigma_8$  in a MOND simulation, one characterising the amplitude of fluctuations of the initial condition and one measuring the strength of fluctuations at the present time. This comes about because of the faster growth of structures in MOND (cf. Sanders 2001; Knebe & Gibson 2004; Llinares et al. 2008), i.e. in order to arrive at a comparable evolutionary stage to a  $\Lambda\text{CDM}$  model at redshift  $z = 0$  with  $\sigma_8 \sim 0.9$  we had to lower the magnitude of the fluctuations to  $\sigma_8 = 0.4$  during the process of generating the initial condition. We acknowledge that this value is incompatible with CMB constraints, at least in the dark matter explanation for cosmic structure formation. MOND, however, is a highly non-linear theory and the simulation presented and used here should be considered as a first toy model for trying to understand structure formation using modified gravity. For more details and elaborate study of the simulation we refer the reader again to Llinares et al. (2008).

In order to perform the analysis presented here we further modified our potential solver to use the MONDian potential  $\Phi_M$  obtained by solving Eq. (4) for the final output at today's redshift  $z = 0$  and our knowledge about the (baryonic) matter density  $\rho$  together with Eq. (5) to obtain the resulting phantom density  $\rho_{\text{ph}}$ .

### 3.3. Locating Density Peaks

Given both the (baryonic) matter density  $\rho$  and the phantom matter density  $\rho_{\text{ph}}$  we determine peaks in both fields. To this extend we smooth the fields on various scales and study spatial offsets in corresponding peaks in relation to the smoothing scale. This is accomplished by exploiting the adaptive mesh nature of the simulation code MLAPM used to generate the simulation in the first place (Knebe et al. 2001; Llinares et al. 2008): the (baryonic) matter is represented by discrete particles whose mass is assigned to a regular grid covering the whole

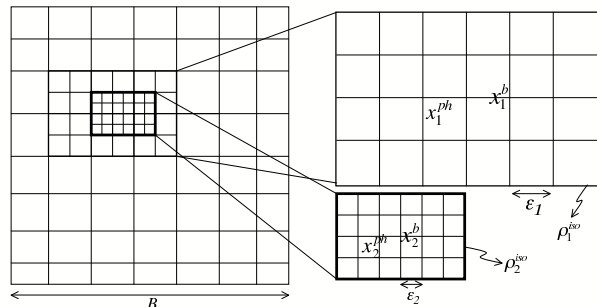


FIG. 2.— Sketch illustrating the definition of the (baryonic) matter density centres  $x_i^b$  on various refinement patches and the corresponding phantom matter peaks  $x_i^{\text{ph}}$ . Note that the boundary of each patch is an isodensity contour  $\rho_i^{\text{iso}}$  in the (baryonic) matter distribution. Due to the nature of the mass assignment of the (baryonic) particles onto each refinement patch we are left with a density field smoothed on approximately the scale of the respective grid spacing  $\epsilon_i$ .

TABLE 2  
SMOOTHING SCALES IN  $h^{-1}\text{kpc}$ .

$L$	$\epsilon_L$ [ $h^{-1}\text{kpc}$ ]
16382	1.95
8192	3.91
4096	7.81
2048	15.63
1024	31.25
512	62.50

computational volume. This grid is then recursively refined in regions of high (baryonic) density according to a pre-selected refinement criterion of 4, 8, or 16 particles per cell. This leaves us with a hierarchy of (nested) refinement patches where the boundary of each such patch defines a unique (baryonic) isodensity contour. The situation is illustrated in Figure 2 where we show an example of two nested refinements embedded within a regular domain grid covering the whole computational volume of side length  $B$ . For each isolated patch we calculate  $x_i^b$  and  $x_i^{\text{ph}}$  by first finding the position of the cell containing the maximum in  $\rho$  ( $\rho_{\text{ph}}$ ); we then use the density (phantom density) weighted average of the 27 neighbouring cells to define  $x_i^b$  ( $x_i^{\text{ph}}$ ). The relevant quantity to be studied below is the difference between the two peaks in the density field

$$D = |x_i^b - x_i^{\text{ph}}|, \quad (6)$$

that obviously is both a function of the smoothing scale  $\epsilon_i$  and the isodensity contour  $\rho_i^{\text{iso}}$ .

### 3.4. Density Peak Offsets

We are primarily interested in the question whether or not there are any (substantial) offsets in the peaks of the (baryonic) matter density field and the corresponding phantom field defined via Eq. (5). For the time being we therefore ignore any relation this offset has with the refinement level it is based upon (cf. Eq. (6)). In Figure 3 we simply plot the cumulative distance distribution  $N(< D)$  normalized to the total number of refinement patches on all levels; we further chose to normalize the distance to

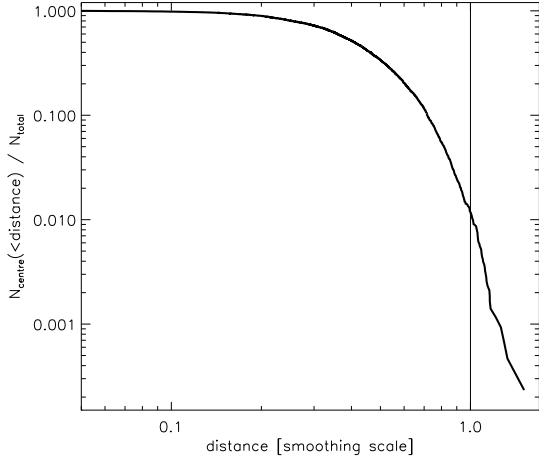


FIG. 3.— The cumulative number distribution  $N(< D)$  of the offset  $D$  between (baryonic) matter density and phantom density. The offset has been normalized to the respective smoothing scale of the refinement patch it is based upon.

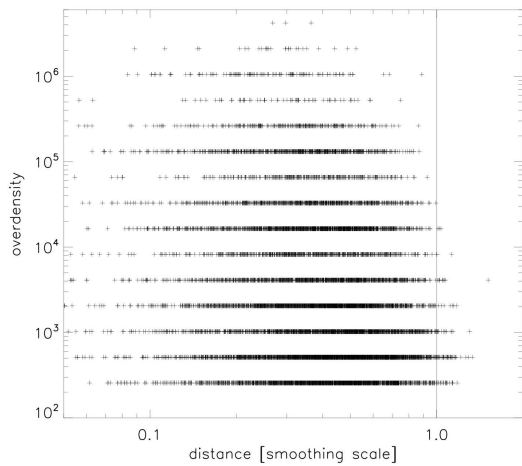


FIG. 4.— The relation between the (baryonic) isodensity level of the refinement patch and the (normalized) offset between matter and phantom density on it.

the respective smoothing scale  $\epsilon_i$  as we consider distances smaller than this scale to be below the resolution limit and hence not credible. The physical values for  $\epsilon_i$  for the grid levels used in our calculations are summarized in Table 2.

While most of the offsets between (baryonic) matter and phantom matter are in fact smaller than the resolution limit there are nevertheless of order 1% instances for which we observe larger (and hence physical) differences!

We like to caution the reader that the same matter peak enters multiple times (at most six times) into Figure 3 (and all subsequent plots below). This is due to the fact that we smooth the same peak using various smoothing scales  $\epsilon_i$  listed in Table 2. However, as we are not interested in the change in offset for a given peak when altering the smoothing scale we can treat them independently.

Even though we just found that there is a small yet

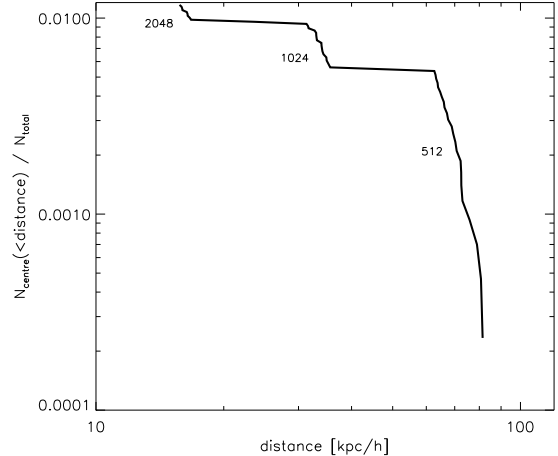


FIG. 5.— Cumulative distribution of isolated patches with an offset  $D > \epsilon_L$  (normalized to the total number of patches). Only patches on grids  $L \leq 2048$  fulfill this criterion and the contribution of these grids to the distribution are marked by the respective  $L$  values given in the plot.

measurable probability of finding an offset between baryonic and phantom density it still remains unclear how this can be interpreted in terms of astrophysical objects. Observationally the edge of an object is primarily defined by a given threshold in (over-)density. This, however, is a natural by-product of our method for calculating  $D$  (cf. Section 3.4). We therefore plot in Figure 4 the dependence of the (normalized) distance  $D$  on the overdensity of the corresponding refinement patch. Recall that the usual overdensity limit for virialized objects in an  $\Lambda$ CDM cosmology at redshift  $z = 0$  is  $\approx 340$  and approximately coincides with our coarsest refinement level.

As the only credible difference in the position of (baryonic) matter and phantom matter peaks are apparent on the lower iso-density levels (i.e. the physically larger refinement patches) one may raise the question whether we calculated the offset for corresponding peaks. A large refinement patch will certainly host several peaks both in baryonic and phantom matter, so how can we be sure to take the difference between matching peaks? Maybe the maximum baryonic density is not at the same position as the maximum phantom density (cf. Section 3.4)? This concern is readily eliminated as the maximum offset observed is no larger than two times the actual smoothing scale, i.e. the peaks lie in two neighbouring grid cells.

So far, we always normalized the offset  $D$  to the respective smoothing scale  $\epsilon_i$ . However, to gain a better and more quantitative feeling for the relevance of our results it appears obligatory to also consider the distance in physical units  $h^{-1}\text{kpc}$ . To this extent we plot in Figure 5 the cumulative distribution of all offsets  $D > \epsilon_L$  larger than the respective smoothing scale in physical  $h^{-1}\text{kpc}$ .<sup>7</sup> Note that only the three coarsest grids (i.e.  $512^3$ ,  $1024^3$ , and  $2048^3$ ) lead to offsets that are larger the smoothing scale; for all finer grids the distance in the (baryonic) matter and the phantom matter peak is below the credibility level given by the smoothing scale. We further ob-

<sup>7</sup> Note that this figure represents a zoom of Figure 3 into the region right of the vertical line and in physical units on the  $x$ -axis now.

serve that the reasonable offsets lie in the range between  $15\text{--}80h^{-1}\text{kpc}$ . We though need to acknowledge that the absolute fraction of isolated patches fulfilling this credibility criterion is below 0.6%. Our simulation therefore has difficulties to accomodate offsets as large as the ones observed.

#### 4. SUMMARY AND CONCLUSIONS

Driven by the observation of offsets in the baryonic and gravitational matter distribution in collisions of galaxy clusters (e.g. Shan et al. 2009) we explore such phenomena in the context of phantom dark matter. This is an interpretation of the MONDian potential (generated purely by baryons) in a Newtonian context, i.e. the MOND potential is used with the standard (Newtonian) Poisson's equation and the resulting right-hand-side source term is understood as a combination of the baryonic matter and some phantom dark matter.

An initial study of (interacting) galaxies in isolation as well as external fields indicated that we should expect to find additional peaks in the distribution of the dynamical mass as opposed to the baryonic mass distribution. However, the strength of these extra peaks varied and the contrast may in some cases be even too low to be observed.

Utilizing a MONDification of the  $N$ -body code MLAPM (Knebe et al. 2001) we set ourselves into the position of calculating both the baryonic and phantom density distributions in a fully self-consistent MONDian cosmological simulation on adaptive refinement patches. We then quantified differences in the peaks of both these fields concluding that the (theoretically predicted) offsets are

too small to be compliant with the observed offsets, at least in the presented incarnation of phantom matter and our MONDian cosmological simulation.

One possible drawback of our applied method is the fact that the isodensity level that define isolated refinement patches are based upon  $\rho_b$  only. However, we compensated for this quibble by adjusting the refinement criterion and subsequently modifying the size of isolated patches; we though could not detect any systematics.

We conclude that our results give support to the idea that neutrino-like non-collisional matter might be responsible for the observed offsets of lensing and X-ray peaks. There are in fact indications by several authors that non-classical neutrinos are required to explain phenomena, such as, cluster lensing (Natarajan & Zhao 2008) or CMB anisotropies (Angus et al. 2009) within the context of (relativistic) MOND. One theory capable of accomodating both these requirements is that of a mass-varying neutrino by Zhao (2008) to be studied more detailed in future work.

AK is supported by the MICINN through the Ramon y Cajal programme. CL and AK further acknowledge funding by the DFG under grant KN 755/2. This work was also carried out under the HPC-EUROPA++ project (project number: 211437), with the support of the European Community - Research Infrastructure Action of the FP7 "Coordination and support action" Programme. XW thanks the support of the SUPA studentship.

#### REFERENCES

- Angus, G. W. 2008, MNRAS, 387, 1481  
 —. 2009, MNRAS, 394, 527  
 Angus, G. W., Famaey, B., & Diaferio, A. 2009, ArXiv e-prints  
 Angus, G. W., & McGaugh, S. S. 2008, MNRAS, 383, 417  
 Angus, G. W., Shan, H. Y., Zhao, H. S., & Famaey, B. 2007, ApJ, 654, L13  
 Bekenstein, J. D. 2004, Phys. Rev. D, 70, 083509  
 Bienaymé, O., Famaey, B., Wu, X., Zhao, H. S., & Aubert, D. 2009, ArXiv e-prints  
 Blanchet, L., & Le Tiec, A. 2009, Phys. Rev. D, 80, 023524  
 Bradač, M., Allen, S. W., Treu, T., Ebeling, H., Massey, R., Morris, R. G., von der Linden, A., & Applegate, D. 2008, ApJ, 687, 959  
 Brownstein, J. R., & Moffat, J. W. 2007, MNRAS, 382, 29  
 Brunton, J.-P., & Esposito-Farèse, G. 2007, Phys. Rev. D, 76, 124012  
 Chen, D.-M., & Zhao, H. 2006, ApJ, 650, L9  
 Ciotti, L., Londrillo, P., & Nipoti, C. 2006, ApJ, 640, 741  
 Clowe, D., Bradač, M., Gonzalez, A. H., Markevitch, M., Randall, S. W., Jones, C., & Zaritsky, D. 2006, ApJ, 648, L109  
 Davis, M., Efstathiou, G., Frenk, C. S., & White, S. D. M. 1985, ApJ, 292, 371  
 de Blok, W. J. G., Bosma, A., & McGaugh, S. 2003, MNRAS, 340, 657  
 Famaey, B., Angus, G. W., Gentile, G., Shan, H. Y., & Zhao, H. S. 2008, in Proceed. of the Sixth International Heidelberg Conference on Dark Matter in Astro- and Particle Physics (DARK 2007), held at the University of Sydney, Australia, 23-28 September 2007, Eds. H. V. Klapdor-Kleingrothaus, G. Lewis, World Scientific, Singapore, ISBN-13 978-981-281-434-0, ISBN-10 981-281-434-5, pp. 393-401, 393-401  
 Famaey, B., & Binney, J. 2005, MNRAS, 363, 603  
 Gentile, G., Famaey, B., Combes, F., Kroupa, P., Zhao, H. S., & Tiret, O. 2007, A&A, 472, L25  
 Halle, A., Zhao, H., & Li, B. 2008, ApJS, 177, 1  
 Hayashi, E., & White, S. D. M. 2006, MNRAS, 370, L38  
 Jee, M. J., White, R. L., Benítez, N., Ford, H. C., Blakeslee, J. P., Rosati, P., Demarco, R., & Illingworth, G. D. 2005a, ApJ, 618, 46  
 Jee, M. J., White, R. L., Ford, H. C., Blakeslee, J. P., Illingworth, G. D., Coe, D. A., & Tran, K.-V. H. 2005b, ApJ, 634, 813  
 Klypin, A., Gottlöber, S., Kravtsov, A. V., & Khokhlov, A. M. 1999, ApJ, 516, 530  
 Knebe, A., Arnold, B., Power, C., & Gibson, B. K. 2008, MNRAS, 386, 1029  
 Knebe, A., & Gibson, B. K. 2004, MNRAS, 347, 1055  
 Knebe, A., Green, A., & Binney, J. 2001, MNRAS, 325, 845  
 Komatsu, E., Dunkley, J., Nolta, M. R., Bennett, C. L., Gold, B., Hinshaw, G., Jarosik, N., Larson, D., Limon, M., Page, L., Spergel, D. N., Halpern, M., Hill, R. S., Kogut, A., Meyer, S. S., Tucker, G. S., Weiland, J. L., Wollack, E., & Wright, E. L. 2008, ArXiv e-prints, 803  
 Li, B., Barrow, J. D., Mota, D. F., & Zhao, H. 2008, Phys. Rev. D, 78, 064021  
 Llinares, C., Knebe, A., & Zhao, H. 2008, MNRAS, 391, 1778  
 McGaugh, S. S. 2008, ApJ, 683, 137  
 Milgrom, M. 1983, ApJ, 270, 365  
 —. 1986, ApJ, 306, 9  
 —. 2007, ApJ, 667, L45  
 —. 2008, ArXiv e-prints  
 Milgrom, M., & Sanders, R. H. 2007, ApJ, 658, L17  
 Moore, B., Ghigna, S., Governato, F., Lake, G., Quinn, T., Stadel, J., & Tozzi, P. 1999, ApJ, 524, L19  
 Natarajan, P., & Zhao, H. 2008, MNRAS, 389, 250  
 Nipoti, C., Londrillo, P., & Ciotti, L. 2007, ApJ, 660, 256  
 Sanders, R. H. 2001, ApJ, 560, 1  
 —. 2005, MNRAS, 363, 459  
 —. 2008, MNRAS, 463  
 Sanders, R. H., & McGaugh, S. S. 2002, ARA&A, 40, 263  
 Sanders, R. H., & Noordermeer, E. 2007, MNRAS, 379, 702

- Shan, H. Y., Feix, M., Famaey, B., & Zhao, H. 2008, MNRAS, 387, 1303
- Shan, H.-Y., Qin, B., Fort, B., Tao, C., & Wu, X.-P. 2009, ApJ, submitted
- Skordis, C. 2008, Phys. Rev. D, 77, 123502
- . 2009, Classical and Quantum Gravity, 26, 143001
- Skordis, C., Mota, D. F., Ferreira, P. G., & Boehm, C. 2006, Physical Review Letters, 96, 011301
- Springel, V., & Farrar, G. R. 2007, MNRAS, 380, 911
- Swaters, R. A., Madore, B. F., van den Bosch, F. C., & Balcells, M. 2003, ApJ, 583, 732
- Wu, X., Famaey, B., Gentile, G., Perets, H., & Zhao, H. 2008, MNRAS, 386, 2199
- Wu, X., Zhao, H., Famaey, B., Gentile, G., Tiret, O., Combes, F., Angus, G. W., & Robin, A. C. 2007, ApJ, 665, L101
- Zhao, H. 2006, ArXiv Astrophysics e-prints
- . 2007, ApJ, 671, L1
- . 2008, ArXiv e-prints, 805
- Zhao, H., Xu, B.-X., & Dobbs, C. 2008, ApJ, 686, 1019
- Zlosnik, T. G., Ferreira, P. G., & Starkman, G. D. 2007, Phys. Rev. D, 75, 044017